Title
Mechanical Overstimulation of Hair Bundles: Suppression and Recovery of Active Motility

Author
KAO, ALBERT

Publication Date
2013

Peer reviewed|Thesis/dissertation

University of California

Los Angeles

Mechanical Overstimulation of Hair Bundles: Suppression and Recovery of Active Motility

A dissertation submitted in partial satisfaction

of the requirements for the degree

Doctor of Philosophy in Physics

by

Albert Kao

2013

Abstract of the Dissertation

Mechanical Overstimulation of Hair Bundles: Suppression and Recovery of Active Motility

by

Albert Kao

Doctor of Philosophy in Physics

University of California, Los Angeles, 2013

Professor Dolores Bozovic, Chair

Hair cells in the inner ear displayed remarkable sensitivity, frequency-tuning, and active amplifying characteristics. Spontaneous oscillations of hair cell bundles observed in several species were hypothesized to be a signature of the amplifying mechanism. Here we brought the system away from its natural state by mechanically overstimulating the hair cell bundle, then observe its recovery. Temporary suppression of spontaneous oscillations after stimulation indicates that there is a negative feedback. Characteristics of the recovery showed that there are two feedback mechanisms working on two different timescales. The shorter timescale, on the order of tens of milliseconds, is consistent with the myosin-based adaptation. The longer timescale, on the order of hundreds of milliseconds, is a feedback mechanism correlated to calcium concentration near the transduction complex. Bundle offset position induced and suppression of active motility are consistent with the variable gating spring model proposed previously. Chapters 3,4,5 are partially adapted from article *Mechanical Overstimulation of Hair Bundles: Suppression and Recovery of Active Motility* PloS ONE 8(3) (2013)

The dissertation of Albert Kao is approved.

Robijn Bruinsma

Felix Schweizer

Dolores Bozovic, Committee Chair

University of California, Los Angeles

2013

To my parents

Table of Contents

List of Figures

Acknowledgments

I want to first thank Professor Dolores Bozovic for giving me the opportunity to work in a lab that is fun and intellectually rewarding. I also would like to thank my fellow coworkers: Elliott Strimbu, Lea Fredrickson, Damien Ramunno-Johnson, Yuttana Roongthumskul, Tracy Zhang, Elizabeth Mills, Bas Meenderink, Yuki Quinones, Michael Levy, Jaehyun Lee, Jiwook Kim and many others who helped me out when I got stuck in my project. Without any of you this thesis would not have been possible.

Vita

2006	B.S. (Physics), National Tsinghua University, Hsinchu, Taiwan
2010	M.S. (Physics), UCLA, Los Angeles, California
2006–2010	Teaching Assistant, Physics and Astronomy, UCLA.
2010–2013	Research Assistant, Physics and Astronomy, UCLA.

Publications

Dynamic State and Evoked Motility in Coupled Hair Bundles of the Bullfrog Sacculus C. E. Strimbu, A. Kao, J. Tokuda, D. Ramunno-Johnson, and D. Bozovic. Hear. Res., 265, 38 (2010)

Effects of the Somatic Ion Channels upon Spontaneous Mechanical Oscillations in Hair Bundles of the Inner Ear D. Ramunno-Johnson, A. Kao, C. E. Strimbu, L. M. Fredrickson-Hemsing, and D. Bozovic. Hear. Res., 268, 163 (2010)

Multiple-Timescale Dynamics Underlying Spontaneous Oscillations of Saccular Hair Bundles Y. Roongthumskul, L. M. Fredrickson-Hemsing, A. Kao, and D. Bozovic. Biophys. J., 101, 603 (2011)

Mechanical Overstimulation of Hair Bundles: Suppression and Recovery of Active Motility A. Kao, S.W.F. Meenderink, and D. Bozovic. PLoS One, 8 (2013)

Low Frequency Entrainment of Oscillatory Bursts in Hair Cells R. Shlomovitz, L. Fredrickson-Hemsing, A. Kao, S.W.F. Meenderink, R. Bruinsma, and D. Bozovic. Biophys. J., 104, 8 (2013)

CHAPTER 1

Introduction to Hearing

1.1 Overview

Hearing is utterly profound and truly remarkable, stemming from the fact that we can sense tiny vibrations of atomic dimensions amidst the thermal jittering of the inner ear. Humans can hear sound as low as 0dB SPL, corresponding to 0.1 nm of vibration at the basilar membrane [52, 16]. The thermal motion in the inner ear was also estimated to be on the order of nanometers [11]; to achieve such remarkable sensitivity, a passive detector is not enough. One way this dilemma could have been solved by nature is to incorporate an active process that distinguishes sound signals from the background noise. When the auditory system is deprived of energy, the sensitivity falls to less than one percent of its normal value [51, 19], demonstrating the significance of the active process. Overall, four phenomena observed and characterized have been attributed to the active process. They are: amplification, frequency tuning, nonlinear compressibility, and spontaneous otoacoustic emissions, elaborated in Figure 1.1. All of these phenomena have been observed in many vertebrate species, suggesting that the active process is not unique to mammals [42], however, in mammals the underlying mechanism may be different from that of non-mammalian tetrapods [3]. For mammals, the active process is suppported by the cochlea and the outer hair cell properties [59]; as for nonmammalian tetrapods, the active process lies in the hair cell bundle motility [17, 44]. Active hair cell bundle motility is a product of the interplay between gating of mechanosensitive ion channels and myosin-based

adaptation motors, which will be expained in more details in Chapter 2. In this study, we observe the modulation and recovery of hair cell bundle motility of the bullfrog sacculus after applying large amplitude stimulation on the hair bundle. In other words, we bring a system from its equilibrium to an extreme state then observe its recovery. The change in hair bundle active motion gives us a glimpse of how the active process responds to mechanical overstimulation.

1.2 Hair Cell

Hair cells are the sensory receptors of pressure wave signals. They are embedded in the sensory epithelium of all auditory and vestibular organs. While hair cells in different species differ in size and shape, many structural and physiological features are similar. Thus, much can be learned from studying hair cells in one given species. Here we take a frog saccular hair cell for example: The hair cell is columnar or flask-shaped, with somatic length 10-20 microns (Figure 1.2). On the apical side of the hair cell, there are 30-60 microvilii packed tightly in a hexagonal pattern that protrude outwards, form a hair bundle (Figrue 1.2). These microvilli, termed strereocilia are circular rods made of actin filaments crosslinked with proteins, and the cells plasma membrane encloses the structure like gloves on fingers [30]. The stereocilium height ranges from 3-8 microns, with diameters around 400 nm. At the insertion point close to the cuticular plate, the stereocilium tapers to a diameter around 100 nm, and the number of actin filaments decreases from several hundreds to a few tens at the pivot. This makes the stereocilia a stiff structure that bends only at its base. In a hair bundle there are 5-10 rows of stereocilia with similar height, stacked in ascending order. Next to the tallest row of stereocilia there is a single true cilium, called the kinocilium. The kinociliums axoneme core consists of an array of paired microtubules [33, 32].

A line drawn from the kinocilium through the center of the hair bundle runs

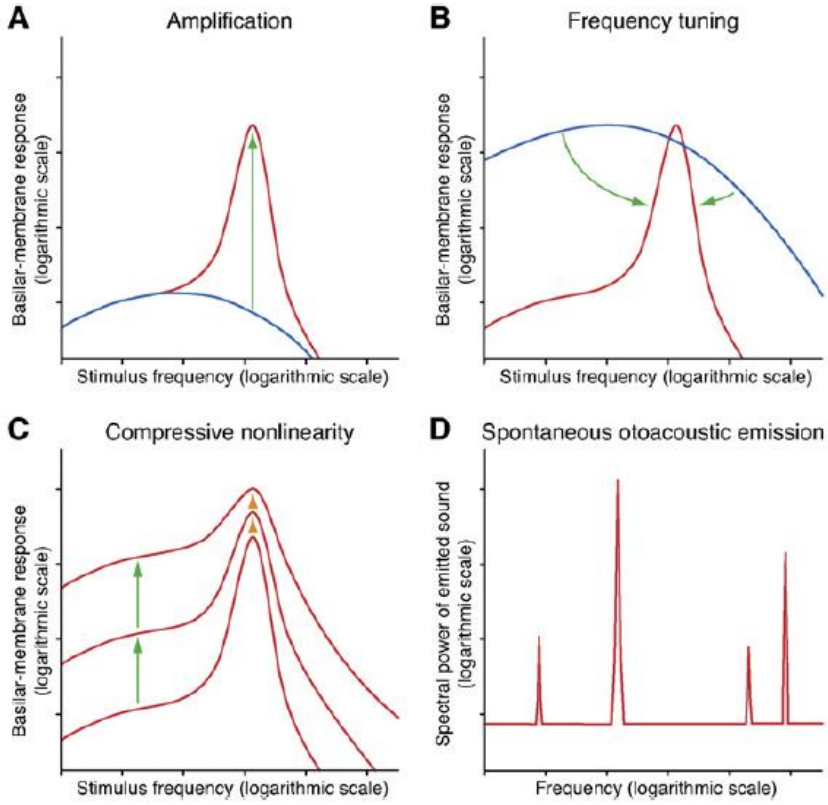

Figure 1.1: Characteristics of the ear's active process (A) An input-output relation for the mammalian cochlea. Amplification by the active process (red) is 100 times greater than the passive response (blue). (B) Basilar-membrane response (red) is sharply tuned to a specific frequency of stimulation than is a passive response driven to the same peak magnitude by much stronger stimulation (blue). (C) Each time the amplitude of stimulation is increased 10-fold, the passive response distant from the natural frequency grows by an identical amount (green arrows). For the natural frequency at which the active process dominates, however, the maximal response of the basilar membrane increases by a factor of about 2.15 (orange arrowheads). (D) Spontaneous otoacoustic emission, the unprovoked production of one or more pure tones by the ear in a very quiet environment. For most species, the emitted sounds differ between individuals. (Figure reproduced from [30])

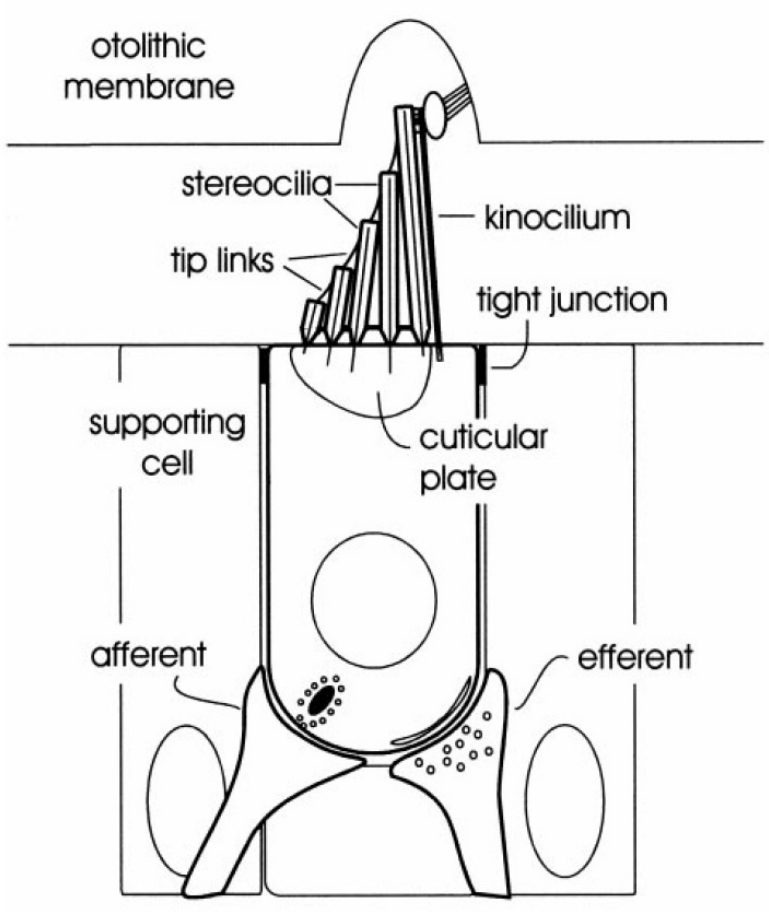

Figure 1.2: Structure of a vertebrate hair cell. The cylindrical hair cell is joined to the adjacent supporting cells by a junctional complex around its apical perimeter, termed tight junction. From the cell's apical surface extends the hair bundle, the mechanically sensitive organelle. When there exists a pressure wave signal, the mass on top of the otolithic membrane will accelerate, then pulls and pushes the stereocilia via the kinociliary connection. (Figure reproduced from [22])

the steepest gradient, and this line forms an axis of symmetry of the hair bundle. Between adjacent stereocilia there are lateral links connecting their entire lengths, so the whole hair bundle moves as one. Near the tip of the stereocilia there is a find braid connection called the tip link, comprising of cadherin 23 and protocadherin 15, reviewed in [54]. The tip link is connected in series with the mechanotransduction complex that transduces mechanical forces into electrical signals [5].

1.3 Mechanoelectrical Transduction

1.3.1 Transduction in a Nutshell

Mechanical stimulation of a hair bundle elicits an electrical response. This is achieved via mechanically sensitive channels near the tip of stereocilia called mechanotransduction (MET) channels. When a hair bundle is deflected, contiguous stereocilia shear against each other and cause the tension of the tip link to increase, which further pulls the in series MET channel, causing it to open. In a resting hair cell, the membrane potential is $\sim$-60 mV. The potential difference and the concentration gradient across the lipid membrane will induce an influx of ions when MET channels open. This flow of ions, called the transduction current, will depolarize the cell by tens of millivolts. Approximately 15 percent of the MET channels are open at rest. Deflection toward the tallest row of stereocilia, defined as the direction of excitation, opens additional channels. On the other hand, a deflection toward the shortest row of stereocilia closes the MET channels that are open and hyperpolarizes the cell. Hair cells respond only to stimulus components parallel to the hair bundles axis of symmetry. A stimulus perpendicular to the symmetry axis evokes no response. The MET channel open probability can be described by a Boltzmann function:

$$P(X) = \left(1 + \exp\left(-z\left(X - X_0\right)/k_b T\right)\right)^{-1} \tag{1.1}$$

Where X is the displacement of the hair bundle, and X_0 is the resting position of the bundle. z is the channel gating force, k_b is Boltzmann's constant, and T is the absolute temperature.Experiments found that displacements less than 100 nm can represent up to 80 percent of the response range. Excitatory deflection (positive direction) increases channel open probability and leads to depolarization of the cells membrane potential. This potential change triggers a biochemical cascade that ultimately causes neurotransmitters release at the base of the soma. Deflection in the negative direction does the exact opposite, decreases the channel open probability, hyperpolarizes the cell and inhibits afferent neuron activity.

The integrity of the tip links is vital to the MET channel gating. If the tip links were broken, for example, by lowering the calcium concentration below 10μM in the surrounding fluid, the transduction current would diminish, for there is nothing that can pull the MET channels open when the hair bundle is deflected [30]. The exact molecular conformation of the MET channels is still under investigation [54], but the locations of the channels were measured with fluorescence imaging. For bullfrog sacculus, the MET channels were found on both ends of the tip links [18], while in mammals the MET channels were found only at the lower end [9].

1.3.2 Transduction Current

The transduction current mostly consists of K^+, the ion that makes up more than 80% of the cations in the endolymph (solution in contact with the apical side of the epithelium) [30]. MET channels are largely non-selective among alkali cations [38]. However, the permeability test showed that the MET channel is more selective for divalent ions over monovalent ions, with Ca^{2+} exhibiting the highest permeability [38]. Ca^{2+} makes up less than one percent of the cations in the endolymph,

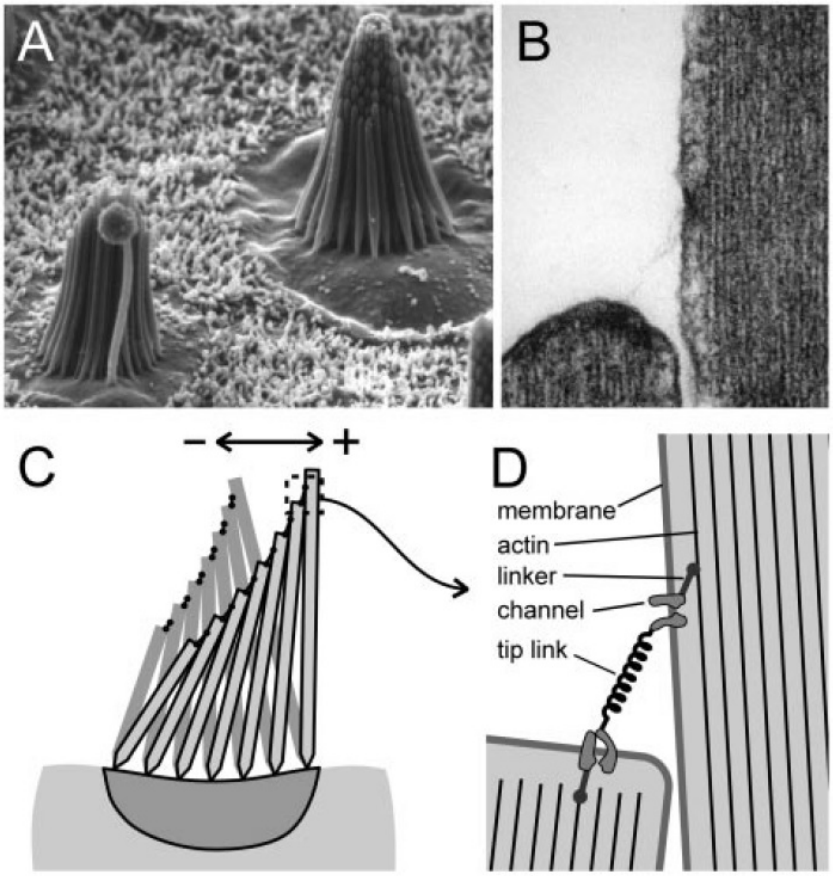

Figure 1.3: Ultrastructure and function of sensory hair bundles. (A) Scanning electron micrograph (2500X) of two hair bundles in the sensory macula of the bullfrog saccule. These bundles are about 8 μmm tall and contain 5060 stereocilia. (B) Transmission electron micrograph (50000X) of the tip of a stereocilium and its adjacent, taller neighbor. Note the fine filamentous tip link extending between the two stereocilia. The tip link is 150-200 nm in length. (C) Schematic diagram of a hair bundle. In this view a bundle deflection to the left is consider a negative stimulus that allows transduction channels to close and a deflection to the right is positive and causes them to open. (D) Schematic diagram illustrating the gating spring model for transduction. When the bundle is deflected in the positive direction the tip links stretch, which would in turn pull directly on the channels and cause them to open. (Figure reproduced from [31])

but unproportionally makes up more than one fifth of the transduction current [38]. Different calcium levels inside the stereocilia lead to different hair bundle dynamics. Calcium ions bind to the MET channel immediately after entry, causing the gating of channel to close [6, 8], and they bind to myosin the motor protein of the transduction complex, modifying the overall tension pulling on the channel [15, 28].

1.3.3 Negative Stiffness of the Hair Bundle

The gating of the transduction channel provides the nonlinearity of a hair bundles mechanical behavior. The stiffness of the hair bundle was measured to be fairly constant for deflection up to 1 micron. However, when a hair bundle is tested in endolymph, standard saline solution mimicking *in vivo* conditions, its displacement-force relation exhibits a nonlinear regime. Over a range of $\sim$50nm centered at the bundles resting position, the bundle displays negative stiffness (Figure 1.4). In other words, within a certain range, the stimulated bundle moves farther than the base of the flexible stimulus fiber used to apply force. Three characteristics were displayed: First, the range of negative stiffness corresponds to that of mechanoelectrical transduction, and shifts with mechanosensitivity. Second, the negative stiffness diminishes after breaking the tip links. Third, blocking the transduction channel eliminates the stiffness change. These findings led us to believe that the negative stiffness regime is associated with the gating of transduction channels [45]. The negative stiffness regime is part of the amplifying mechanism. Small inputs within that are within the range of negative stiffness will be amplified, for the bundle movement exceeds the external stimulus.

1.4 Adaptation

1.4.1 Adaptation in a Nutshell

Sensory adaptation is the decay of a sensory response to a sustained stimulus. Such an effect is common for a system to maintain sensitivity for detecting new stimuli (Figure 1.5). The decline in the receptor current is the result of reclosure of transduction channels. Hair cell adaptation has been found to be associated with a shift in the current-displacement I(X) relation in the direction of the applied deflection, thus bringing the channel open probability closer to its resting values. However, adaptation is not complete. The extent of adaptation was 60 - 80 % of the magnitude of the bundle deflection [55]. In normal conditions, the receptor current reaches steady state in 150 ms, with a decay time constant of 20-30 ms when fitted to an exponential function. The sensitivity range of a hair bundle has a limit of up to $\sim$ 500 nm. If the hair bundle deflection is above 500nm, the receptor current saturates.

1.4.2 Myosin 1C as the Adaptation Motor

In order to achieve adaptation, a feedback system that is stable and can be repetitively modulated must exist. The model for such mechanism was proposed to be a myosin-actin complex. The model for such a mechanism is described as the movement of the gating spring/tip link insertion on the side of the stereocilium (Figure 1.5). During positive deflections the adaptation process promotes slipping of the tip link insertion along the stereocilium, reducing the stretch of the tip link, tension on the gating spring and the channel open probability P(X). During negative bundle deflections, the adaptation process involves climbing of the tip link insertion upward along the strereocilium, restoring transduction channel open probability and the tension in the gating spring. It was speculated that the moving element is myosin, moving along the actin skeleton of the stereocilium.

Myo1C was found in the tip of the stereocilia, and was assumed to be the adaptation motor [26]. Structural and biochemical experiments estimated the number of Myo1C molecules to be a few hundred [27]. Myo1C structure consists of three domains: head, neck, and tail. The head is actin binding and ATP consuming, and responsible for generating the two-step power stroke. The neck region has six calmodulin binding IQ domains. Calcium modulates the activity via calmodulin by stiffening the neck region and controlling the step size [1]. The tail is anionic and phospholipid binding, which is used for cargo transport [41].

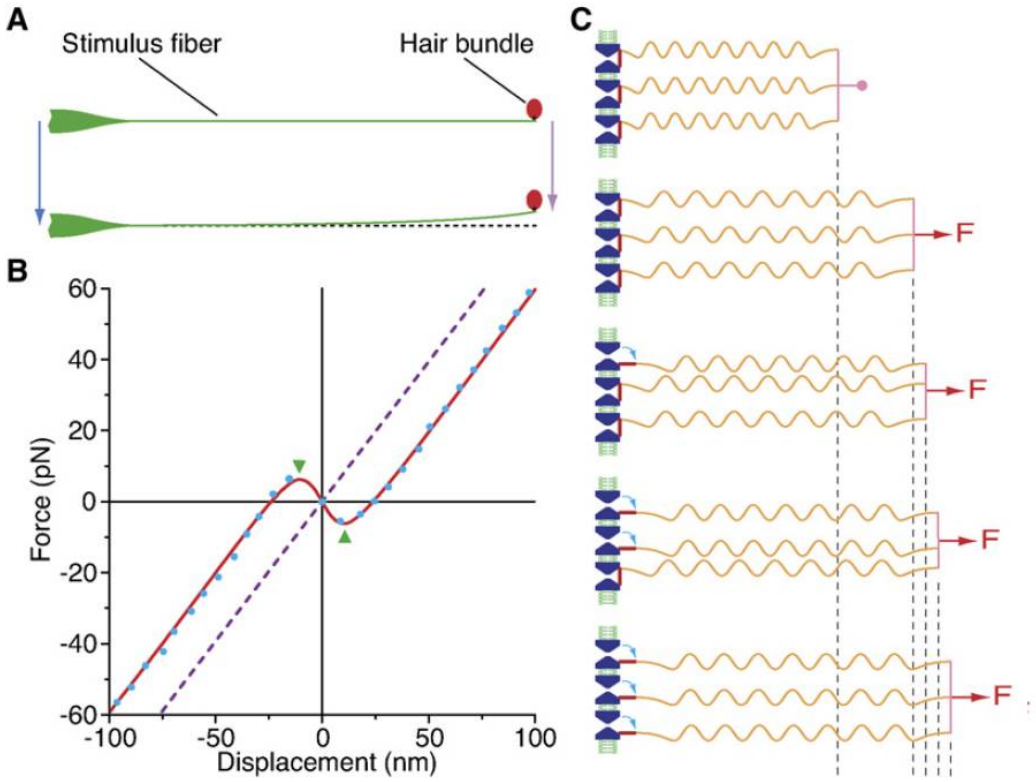

Figure 1.4: Nagative hair bundle stiffness. (A) The mechanical properties of a hair bundle are assessed by connecting its top to the tip of a glass stimulus fiber. (B) The displacement-force relation obtained from a spontaneously oscillating hair bundle (blue points and fitted red curve) differs strikingly from that of a linearly elastic object. The unrestrained bundle cannot remain in the negative stiffness region (green arrowheads). (C) The coordinated gating of mechanoelectrical-transduction channels explains the hair bundles negative stiffness. (first diagram). When a constant force F is applied to the parallel array of channels, the three gating springs are stretched to an identical extent (second diagram). As one channel opens, the movement of its gate partially relaxes the associated gating spring (third diagram). Because the gating springs for the two remaining channels consequently bear additional tension, either of those channels is more likely to open as well (fourth diagram). (Figure reproduced from [30])

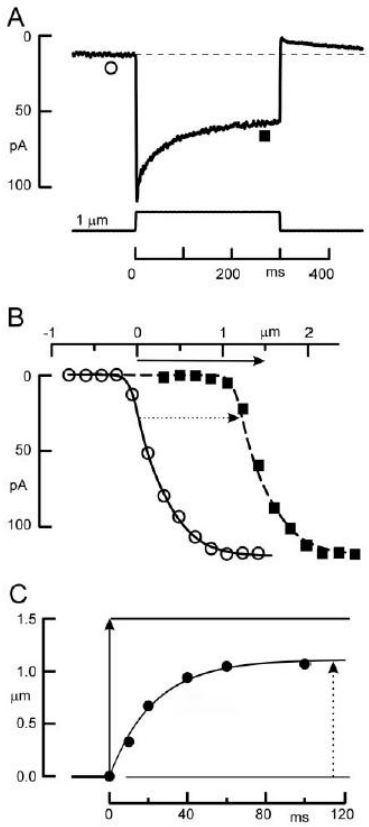

Figure 1.5: Properties of adaptation in a hair cell. (A) Transduction current evoked by deflecting the hair bundle. The current declines in response to a step deflection. (Circle, Square) Time points at which the I(X) curves in B were acquired. (B) The I(X) relation shifts in the direction of the applied stimulus. Circles, The peak currents plotted vs. bundle deflection beginning from a resting bundle position. Squares, An I(X) relation that was measured near the end of 300-msec, 1.5 μm bundle deflection similar to that shown in A. (C) Magnitude of the I(X) shift as a function of time. The position of I(X) curves such as those in B were measured at several time points after the onset of a 1.5 μm deflection. Fitting these data with an exponential function indicated that the curve shifted with a time constant of 23 msec. Solid arrow indicates magnitude of the stimulus; dashed arrow shows final magnitude of the I(X) shift. (Figure reproduced from [31])

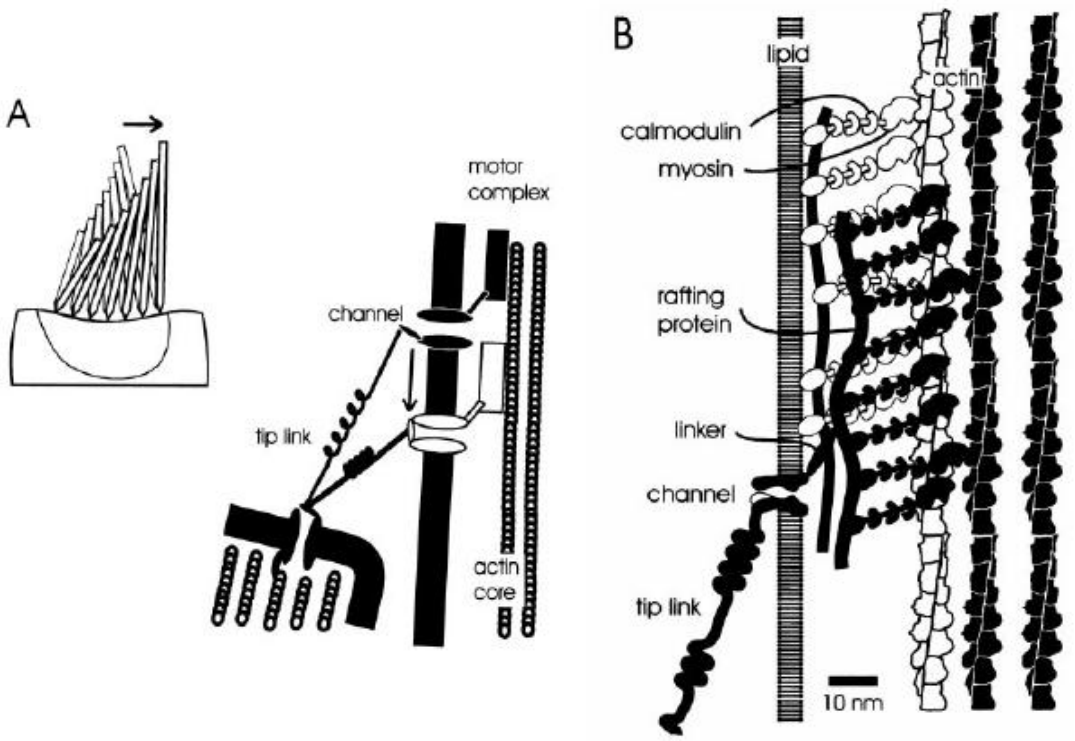

Figure 1.6: (A) The motor model of transducer adaptation. Positive deflection of the bundle (arrow, inset) initially extends the tip link, increasing the open probability of the transduction channels. The increased tension and Ca^{2+} influx promote slipping of the motor complex relative to the actin core. The complex is connected to the transduction channel and tip link and drags them along (vertical arrow). (B) Detail of transduction/adaptation complex. The complex is shown in two conditions with different predicted adaptation rates. (white) All the myosin heads are attached to the actin; (black) with few myosin heads coupled to actin, the complex generates less resistance to be pulled by an extended tip link and slips faster. (Figure reproduced from [22])

CHAPTER 2

Spontaneous Oscillation of Hair Bundles

2.1 Overview of Active Bundle Motility

The inner ear needs to amplify mechanical signals to achieve sensitivity and frequency tuning. All inner ear organs are immersed in a viscous environment that dissipates energy, so the amplifier in the inner ear has to provide energy on a cycle-by-cycle basis to enhance the mechanical input. In mammals, the source of the cochlear amplifier was not yet been fully determined, but the consensus in the field is that the outer hair cells perform amplification by cellular length changes in response to the transmembrane voltage variations [37]. On the other hand, for species that do not possess outer hair cells, the amplification must come from other means. The amplifier of nonmammalian tetrapods is active hair bundle motion as it was observed in several species [23, 45]. This active bundle motion, termed spontaneous oscillations is the interplay between negative stiffness of the bundle and the adaptation mechanism. One important condition for the spontaneous oscillations to occur, is that the ionic surroundings in contact with the apical and basolateral surfaces of the sensory epithelium need to be similar to their physiological levels; i.e. endolymph (high $[K^+]$ solution) must be bathe the hair bundle, while perilymph (high $[Na^+]$ solution) must bathe the hair cell body. Moreover, spontaneous oscillations have not been observed in isolated hair cells, as there are no supporting cells in contact to keep normal metabolism. In bullfrog sacculus, the oscillations displayed in each hair cell has its own characteristic frequency. The oscillation frequency for frog saccular hair cell bundles ranges between 10-

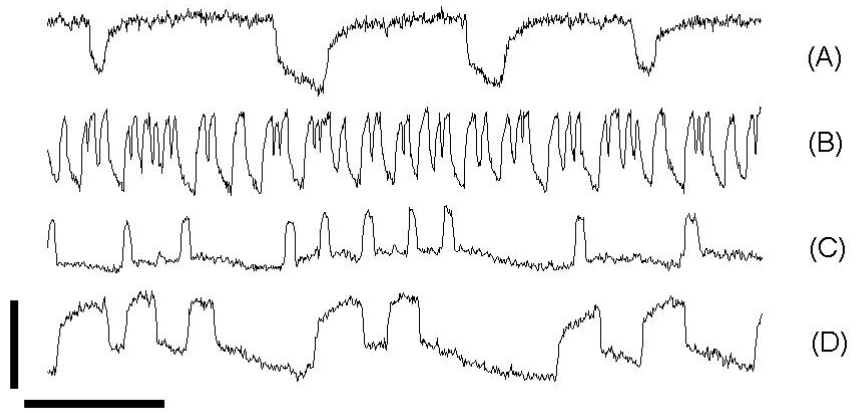

Figure 2.1: Varieties of spontaneous hair bundle oscillations. (A)-(D) Various spontaneous oscillation profiles. Scale bars equal 100 nm and 200 ms respectively.

100Hz, with peak-to-peak amplitude up to 100nm (Figure 2.1). If a bundle is mechanically stimulated at its characteristic frequency, the hair cell displays its largest response, supporting the view that hair bundle motility is the amplifier at the sensory receptor level [24].

2.2 Extracellullar Calcium affects Oscillatory Motion

Increasing the extracellular calcium concentration in contact with the apical surface makes spontaneous oscillations of the hair bundles faster and smaller until they are suppressed; lowering the extracellular calcium concentration with calcium chelators gives the opposite effect. For each cycle of the spontaneous oscillation there are two kinds of movements that work on different time scales. One is a movement that represents relaxation, working on the order of tens to hundreds of milliseconds. The other kind is a rapid stroke which is only a few to a few tens of milliseconds (Figure 2.1). For every half cycle, a fast stroke is followed by the slower relaxation in the same direction. The relaxation motion is due to the myosin motor complex movement along the actin filaments, and the rapid stroke

is related to the transduction channel opening or closing [30]. Calcium ions mediate both processes by modulating activity of the adaptation motor and changing the ion channel open probability [14]. Under normal condition, higher calcium concentration in the endolymph increases the rate of channel opening and closing, making the overall spontaneous oscillation frequency higher. Moreover, the adaptation rate is faster with high calcium concentration. In *in vitro* experiments Myosin 1C was found to climb at up to three times faster in high calcium than in low calcium solutions [27]. With control of the calcium near the transduction complex one can control the bundle movement. Transepithelial currents applied to the sacculus can modulate hair bundle active motion [7]. Calcium is driven in and out of the stereocilia by the voltage signal. The phase difference of the signal and the bundle motion depends on the bundle parameters, but the signal and motion are always phase-locked for stimulus near the characteristic frequency (Figure 2.4). If the extracellular calcium concentration was raised above 1mM or lowered below 100μM, the spontaneous oscillations diminish.

2.3 Regulation of Calcium in Stereocilia

From Figure 2.2 and 2.3 we see that Ca^{2+} concentration near the transduction complex plays an important role in hair bundle motility. Calcium not only modulates the Myosin 1C power stroke cycle, but also induces MET channel closure. Almost every aspect of the spontaneous oscillations are affected by calcium [30]. There are four main regulatory mechanisms that maintain stereociliary calcium homeostasis: Ca^{2+} diffusion; Ca^{2+} extrusion by PMCA pumps, Ca^{2+} binding to fixed buffers; Ca^{2+} binding to mobile buffers. Precise parameters are not easily accessible, and the measurements of the mechanisms were done on enzyme-treated isolated hair cells that had no supporting cells. Nonetheless, the parameters shed light on the dominant calcium regulatory activities inside the hair cell. The esti-

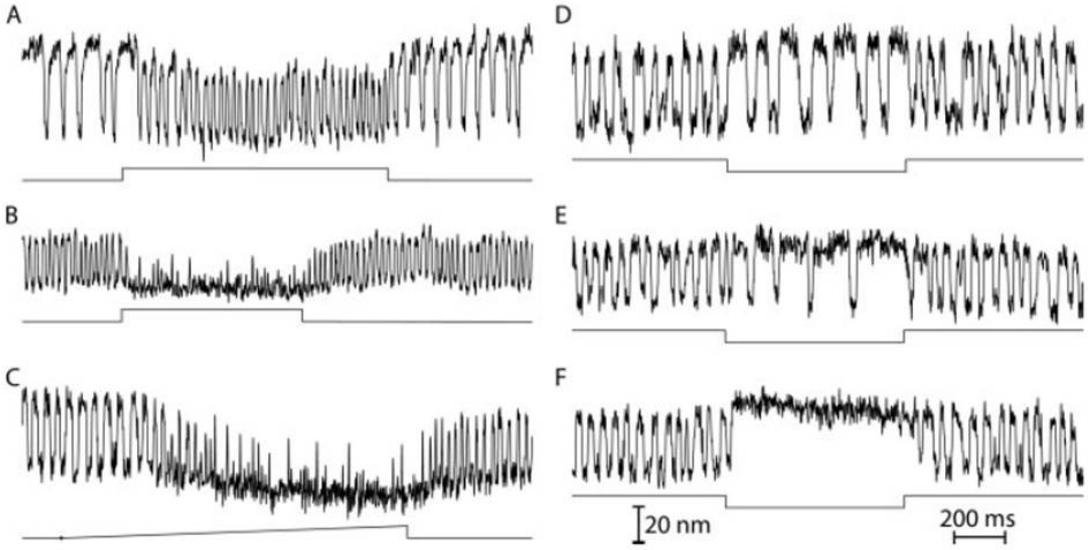

Figure 2.2: Effect of extracellular Ca^{2+} concentration on spontaneous hair bundle oscillation. (A) The increased Ca^{2+} concentration offset the bundle and decreased the rms magnitude of the movement. The frequency of oscillation also rose, primarily by shortening of the positive phase of motion. The 1 sec iontophoretic pulse is indicated below (B) Although the largest Ca^{2+} ejections suppressed rhythmic hair bundle activity, fast, erratic movements remained. (C) Ca^{2+} expelled by a ramp of iontophoretic current initially accelerated and eventually suppressed spontaneous bundle oscillation. (D) An 0.7-sec iontophoretic pulse of ATP decreased the local Ca^{2+} concentration around a hair bundle, causing a net movement of 5 nm and prolonging the positive phase of oscillation. (E) A greater reduction of the Ca^{2+} concentration. F, Even greater reduction of the Ca^{2+} concentration suppressed the oscillation. (figure reproduced from [48])

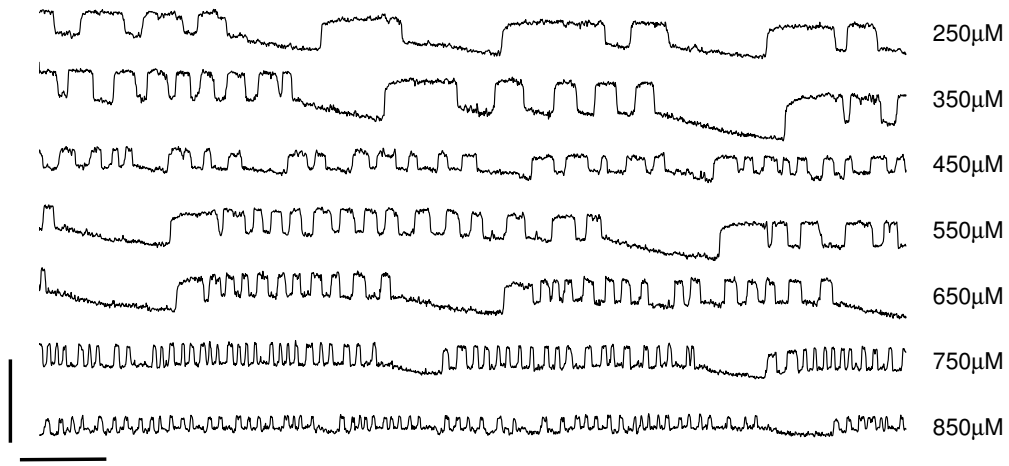

Figure 2.3: Spontaneous oscillations exhibited by a hair bundle under various calcium concentrations. Increasing levels of calcium were introduced into the endolymph, indicated to the right of the traces. The oscillation amplitude decreased and the frequency increased with higher calcium concentrations. Horizontal and vertical scale bars equal 0.2 s and 200 nm respectively.

mated free calcium concentration after bundle deflection is on the order of 1μM near the transduction complex [27, 10]. Near the bottom of the stereocilia, the calcium signal is only above the noise level, and the rise to its peak value comes 10ms after that of the top of the stereocilia, indicating mobile and fixed buffers plays a huge role in spatially restricting the spread of Ca^{2+} [39]. Plasma membrane Ca^{2+} ATPase molecules provide the only known Ca^{2+} extrusion mechanism in the hair bundle. The pumps reduce the Ca^{2+} concentration below that of the soma with a peak current of 1pA during bundle deflection [39]. Without any of the mechanisms mentioned above, free calcium data cannot be sufficiently explained. Taking all information into account, the calcium concentration near the transduction channels close to the adaptation motors was estimated to double after bundle deflection, on the order of micromolars [27]. After transduction channel closure, buffers and diffusion will succinctly bring the calcium level back to steady state within 100ms. At the base of the stereocilium, the calcium level barely changes with stimulation.

2.4 Hopf Bifurcation

The four characteristics of hearing, which were introduced in Figure 1.1, were discovered independently, however, there may be a common underlying mechanism [40]. A simple mathematical model can display all four features if the system operates near a particular type of instability called a Hopf bifurcation. Hopf bifurcation is not the only model that can describe all four phenomena, but it should be the most simple one. A bifurcation is said to occur when a small change in the value of one parameter, the control parameter, causes a qualitative change in the systems behavior. At the critical point of a Hopf bifurcation a tiny change in the control parameter shifts a system between two regimes. On one side of the bifurcation the system is unstable, it oscillates spontaneously without any input. On the

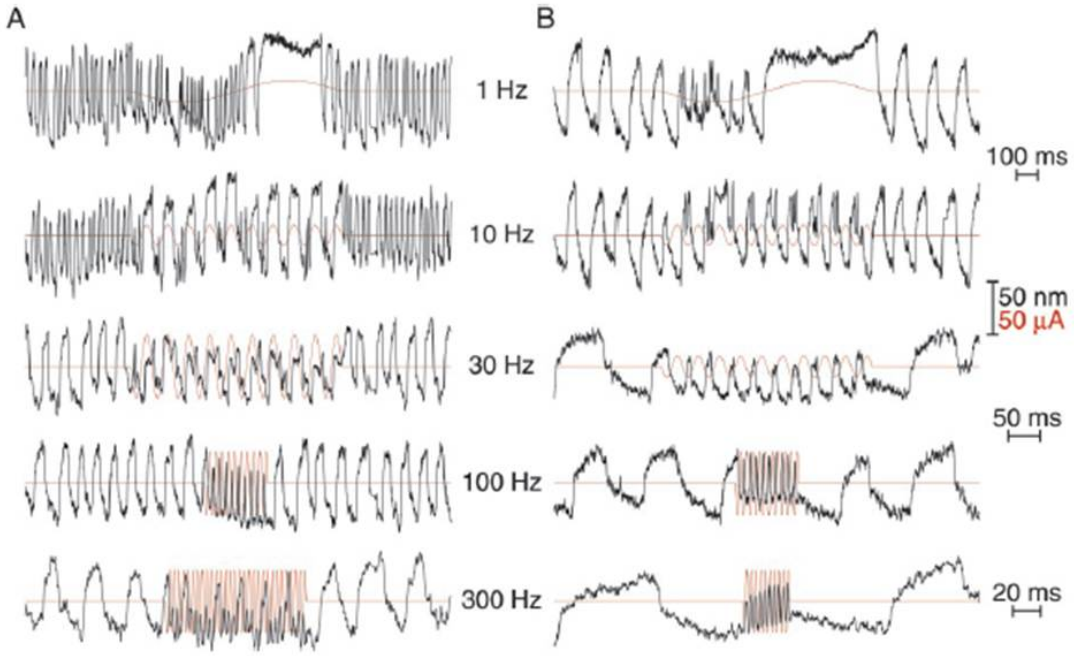

Figure 2.4: Response of active hair bundles to stimulation by sinusoidal transepithelial current. (A) Before stimulation, a hair bundle oscillated spontaneously at 35 Hz. During negative stimulation at 1 Hz, the bundle displayed faster and smaller oscillations with occasional omissions; the positive stimulus phase slowed and eventually blocked oscillatory movements. Similar responses occurred during stimulation at 10 Hz. At 30 Hz, slightly below the natural frequency of the cell, the response comprised phase-locked movements adorned with complex spikes. At 100 and 300 Hz, the response was essentially out of phase with the stimulus. During a 300-Hz stimulation, spontaneous bundle oscillations resumed, superimposed on the rapid, phase-locked response. (B) The hair bundle of a second cell oscillated spontaneously at 8 Hz. Although electrical stimulation evoked responses similar to those in A, the transition from the low- to the intermediatefrequency regime of responsiveness occurred at a frequency 10 Hz. (figure reproduced from [7])

other side the system can amplify its input while remaining stable. [30]. Analysis indicates that a system operating on the stable side of a Hopf bifurcation exhibits the first three characteristics of the ears active process: amplification, frequency selectivity, and compressive nonlinearity. The spontaneous otoacoustic emission emerges on the unstable side of the Hopf bifurcation, where limit-cycle oscillations exist. For optimal sensitivity, the ear must poise itself close to the critical point. Negative feedback of a signal representing excitability can achieve this condition. In our following studies, we perturb the hair bundle away from its sensitive regime, namely the regime where it displays spontaneous oscillations. After releasing from its perturbed state, which does not oscillate, the hair bundle will the slowly recover back to oscillating. The time course for the bundle to return to an oscillatory state represents the time for negative feedback. With the time scale determined, we can better figure out which of the adaptation mechanisms are responsible for the feedback after mechanical overstimulation. Thorough discussions about the Hopf bifurcation feedback and hearing can be found in [20, 12].

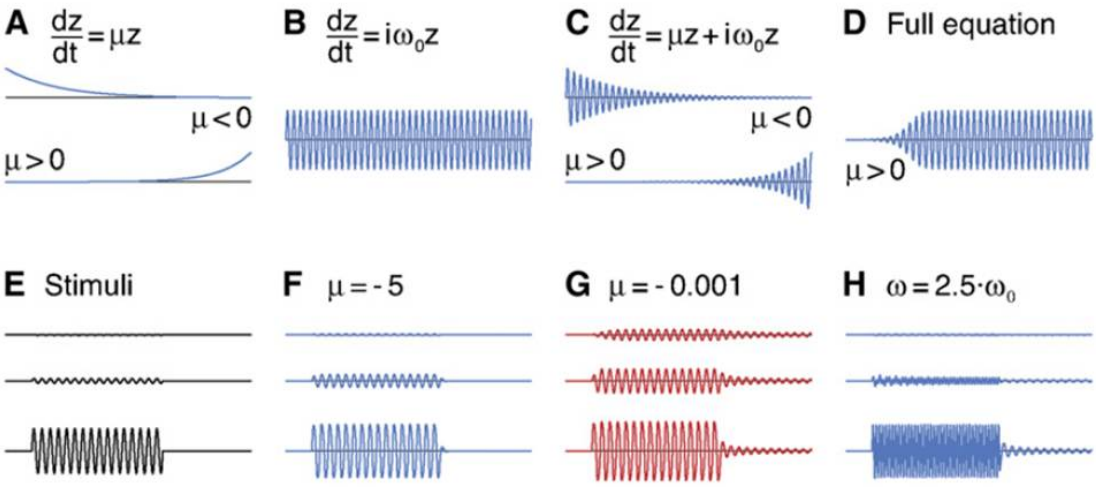

Figure 2.5: Properties and Consequences of the Hopf Bifurcation (A) The real part of the solution for the simplified equation with only the initial term on the right displays exponential decay for negative values of the control parameter m or exponential growth for positive values. (B) Including only the second term on the right leads to solutions that are sine and cosine waves at the natural frequency μ_0.(C) Combination of the initial two terms produces oscillatory solutions that decline or grow exponentially. (D) For positive values of the control parameter, the complete equation yields spontaneous limit-cycle oscillation at the natural frequency μ_0. This unforced activity may underlie spontaneous otoacoustic emission. (E) A system driven with stimuli of realtive amplitudes 1, 10, and 100 units (top to bottom). The system undergoes a Hopf bifurcation. (F) When the dynamical system operates far from the bifurcation, its passive responses at the natural frequency are nearly linear reflections of the three stimuli. (G) When functioning near the Hopf bifurcation and stimulated at the natural frequency, the same system displays profound amplification. (H) Even at the bifurcation, the systems tuning is evident from the weak amplification of stimuli whose frequency differs from the natural frequency μ_0. (Figure reproduced from [30])

CHAPTER 3

Methods

3.1 Biological Preparation

Experiments were performed on *in vitro* preparations of the sacculus, excised from the inner ear of the North American bullfrog (*Rana catesbeiana*). Dissections were carried out in artificial perilymph to extract the saccular macula. After extraction of the sensory epithelium, it was then mounted in a two-compartment chamber, with hair cells exposed to artificial perilymph and endolymph on the basal and apical sides respectively. The solutions were made to mimic the ionic conditions in the sacculus; for perilymph, it contained (in mM) 110 Na^+, 2 K^+, 1.5 Ca^{2+}, 113 Cl^-, 3 d-glucose, 1 sodium pyruvate, 1 creatine, 5 HEPES; and for endolymph: 2 Na^+, 118 K^+, 0.25 Ca^{2+}, 118 Cl^-, 3 d-glucose, 5 HEPES. Both solutions, with pH 7.3 and osmolarity 230 mmol/kg, were oxygenated for $\sim$ 10 minutes prior to use. The overlying otolithic membrane was removed from the epithelium with an eyelash tool following a 7–8 minute enzymatic dissociation with 15μg/mL Collagenase IV (Sigma Aldrich). Active spontaneous oscillation was observed in hair bundles after decoupling from the membrane, and could be maintained for several hours post dissection.

3.2 Detection of Hair Bundle Motility

Preparations were imaged in an upright optical microscope (Olympus B51X) with a water immersion objective (20X, 0.95 N.A.) and illuminated with a X-Cite

120W halogenide lamp. Images were further magnified to ∼400X and projected onto a high-speed Complementary Metal Oxide Semiconductor (CMOS) camera (Photron FASTCAM SA1.1). The motion of the hair bundles was tracked with software written in MATLAB (The MathWorks). A horizontal line scan was taken through the image in each frame, and a Gaussian distribution is fit to the intensity profile of the bundle to extract the center position. To improve the signal-to-noise ratio, 11–15 vertically adjacent pixel rows, chosen such that the brightest pixel is at the center, were tracked and averaged. Time-dependent traces of the movement were then obtained by plotting the extracted center position of the bundle for each frame of the record. The noise levels in these recordings were ∼3–5 nm.

3.3 Mechanical Overstimulation

We applied prolonged mechanical overstimulation to bring the cell away from its equilibrium state. Glass fibers were pulled with a micropipette puller (P97, Sutter Instruments), with an additional rod ∼2-3 μm in diameter fabricated at a 90 degree angle using a home-built puller. The fibers were mounted on a piezoelectric stimulator (P-150 Piezo Jena) and positioned in the vicinity of the hair bundle with micro-manipulators. Step signals were generated with a function generator (Tektronix; model AFG 3022), low-pass filtered with an eight-pole Bessel filter at 100 Hz (Krohn Hite; model 3382), and sent to the piezoelectric amplifier. CMOS camera recording was synchronized with cessation of stimulus. Deflection imposed on the bundles was measured from the video recordings by subtracting the bundle position under deflection from the original position. Only records where no adhesion was observed between the probe and the bundle were included in the analysis.

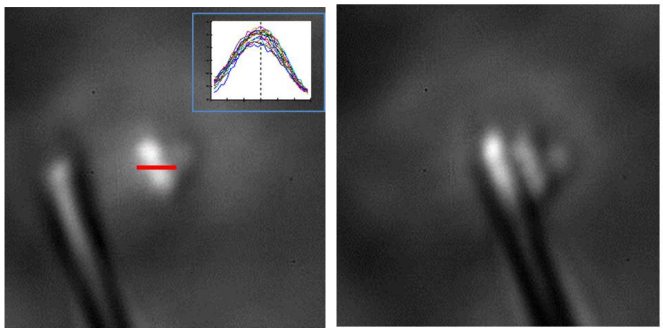

Figure 3.1: Example of hair bundle position analysis. A glass probe was used to deflect a hair bundle. Bundle displacement was determined by fitting a Gaussian function to the light intensity profile of the pixel row at the bundle tip, indicated by a red line, and find its center. Red line is 1 μm in width, also serves as a scale bar.

3.4 External Calcium Concentration and Extrusion Blockers

Mechanical deflection was applied and a fixed amplitude and duration, under different ionic conditions. Between recordings, calcium was added into a measured quantity of endolymph bathing the apical surface of the preparation, with mechanical over-stimulation repeated at each of the enhanced levels of calcium in the medium. For measurements at reduced calcium concentrations, the endolymph in the top compartment was fully replaced, with the fluid exchange performed using a peristaltic pump. Equivalents of 1mL volumes of the top solution were exchanged.

For one set of experiments, we blocked the calcium extrusion pumps with carboxyeosin diacetate succinimidyl ester (CEDA; Sigma Aldrich). The reagent was dissolved in dimethyl sulfate oxide (DMSO), then diluted to concentrations of 1-10 μM in endolymph. The final concentration of DMSO is 0.2% in endolymph.

CHAPTER 4

Results

4.1 Fitting the Data

Recordings from 57 saccular hair cell bundles (N = 34 frogs) that exhibited robust spontaneous oscillations are used for analysis. Large deflection of hair bundles greater than 1 μm in the positive direction consistently led to a temporary suppression of the spontaneous oscillations following the stimulus (Figure 4.1). Additionally, bundles showed an offset in their position that decreased with time. To minimize the effects of cell rundown, we only included those hair cells in the analysis that showed robust bundle oscillations of more than 4Hz prior to the first stimulus protocol. In addition, the spontaneous bundle motility had to recover to more than 3Hz, or the hair bundle is determined to be too weak for additional recordings.

Several parameters were extracted from the time-dependent traces $x(t)$ (Figure 4.1). First, the trace was bandpass-filtered (0.5–150Hz), and candidate oscillations were identified as large (> 10 nm) hair bundle movements toward the kinocilium. Next, the maximum slopes leading to and following after each candidate oscillation were calculated. If the absolute value of both slopes exceeded 1 nm/ms ($|dx/dt| >$ 1 nm/ms), the excursion was considered an oscillation of the bundle.

To extract the characteristic times of the recovery of the bundle in the closed-channel position, the identified oscillations were removed from the trace, and the

remaining data were fitted to the function:

$$X(t) = C + A_1 \exp\left(\frac{-t}{\tau_1}\right) + A_2 \exp\left(\frac{-t}{\tau_2}\right), \text{with } \tau_1 > \tau_2 \tag{4.1}$$

Besides providing the two time constants (τ_1, τ_2), the fitted function was used to calculate the time of recovery to the steady state (T_{ss}; the first moment $dX/dt > -0.02$ nm/ms after cessation of the stimulus), and the initial offset in the bundle position after stimulation (the bundle's postion at the end of the recording, $X_0 = X_{t=0} - X_{t=T}$, where T is the duration of the record). Based on the detected oscillations, we define T_q as the starting time of the first oscillation, with $X_q = x(T_q) - X_{t=T}$ being the corresponding position of the bundle.

4.2 Suppression of Spontaneous Oscillation

In approximately 100 cells studied, deflections above $\sim$1 μm and longer than 0.1 seconds consistently led to a suppression of spontaneous oscillation, with the bundles rendered quiescent following cessation of the stimulus. The quiescent states typically lasted between hundred milliseconds and few seconds. Immediately post stimulus, the bundles displayed an initial offset in the positive direction. A subsequent slow movement in the negative direction was a consistently observed feature. As the offset in the average position was reduced, spontaneous oscillation resumed.

We note that hydrodynamic drag cannot account for the slow movement in the negative direction observed during the quiescent state. Based on estimates of a hair bundle's stiffness and viscous drag coefficient [48], the return to original position upon release from 1 μm deflection should occur with sub-ms delay. We verified this by imposing brief pulse-like stimuli (Figure 4.2). Offset in the bundle position, induced quiescence, and the gradual recovery were only observed after prolonged exposure to a stimulus.

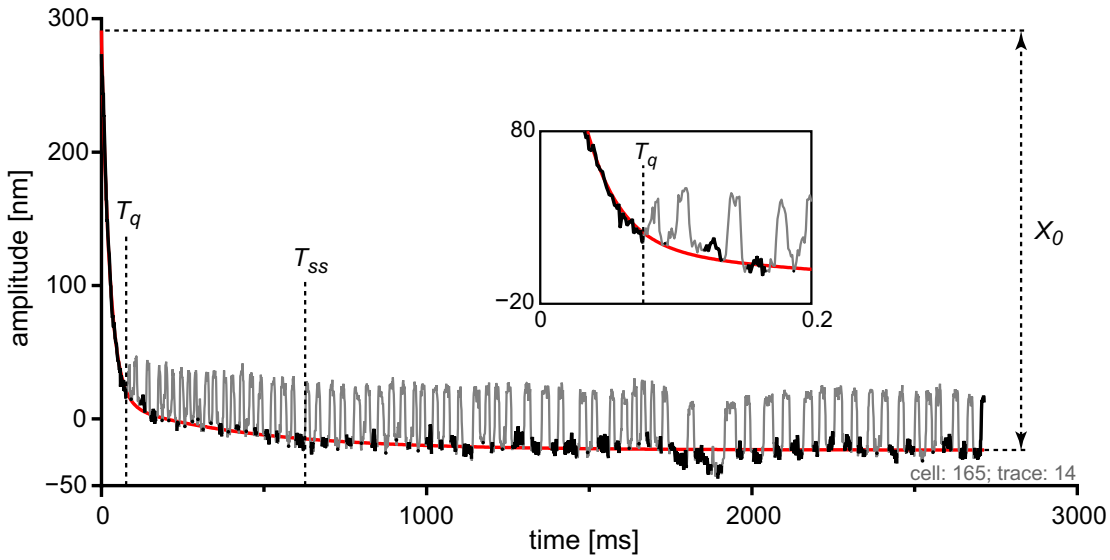

Figure 4.1: The gray/black curve shows the position of the bundle, with motion towards the kinocilium being positive. An automatic routine detected bundle oscillations (gray) from which the onset time of the first oscillation Tq was determined. A sum of two exponentials (see Eq. 4.1) was fitted to the bundle's position in the closed state (black), thus ignoring the oscillations. From the fit (red: $X(t) = -23.4 + 37.4 \times \exp\left(\frac{-t}{418.6}\right) + 227.1 \times \exp\left(\frac{-t}{25.1}\right); r^2 = 0.97$), the time to reach steady state Tss was calculated as the time for which its derivative first reached -0.02 nm/ms. It was also used to calculate the bundle's total offset Xo, defined as the difference between the position at t=0 and the end of the recording. The stimulus was a one-second DC offset in positive direction.

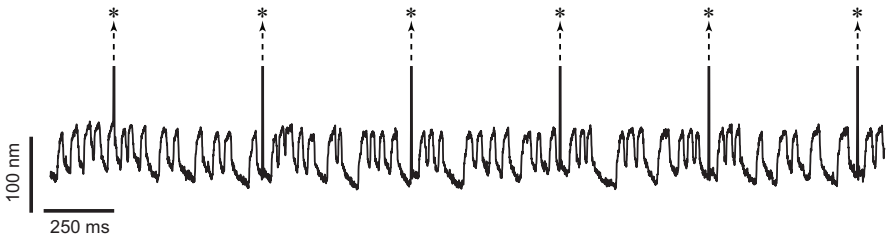

Figure 4.2: Hydrodynamic drag is not the cause of delayed recovery. A spontaneously oscillating hair bundle was mechanically stimulated every 500 ms with a large (1μm), and brief (5-ms) pulse (asterisks). Recovery from such transient, large offsets is fast, indicating that hydrodynamic effects play only a marginal role in the observed slow recovery that follows longer stimulations. In the analysis of all data, the first 5 ms following each stimulus are excluded, to further minimize the hydrodynamic effects.

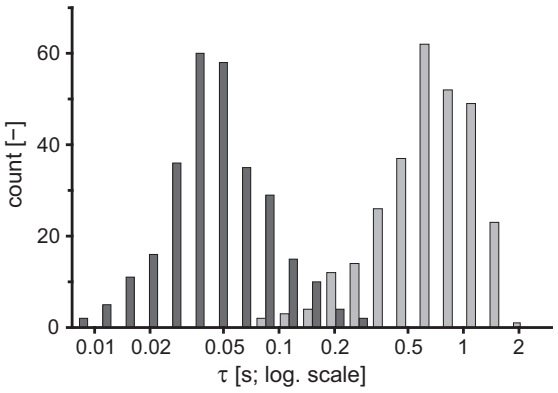

Figure 4.3: τ values of the recovery. The slow component of the bundle movement following a prolonged deflection was fitted with the sum of two exponentials (Student's t-test, p<0.001), yielding two time constants $\tau 1$ and $\tau 2$, with $\tau 1 > \tau 2$. For 282 recordings (of $N = 411$), a good fit was obtained. The two time constants are represented in the histogram by different shadings of gray.

4.3 Multiple Timescales of the Recovery

The result that the relaxation of hair bundles is best described by the sum of two exponentials suggests that the adaptation following a prolonged excursion involves at least two processes that operate on different time scales. However, the two time constants show an average correlation coefficient of 0.47, which tells us that the two mechanisms affect each other. The spread of two tau values are shown in Figure 4.3, with different stimulus duration and stimulus amplitude combined. The shorter of the time constants was in the range ∼20-50 ms, consistent with myosin-motor dynamics. The second time constant was significantly slower ∼0.5-1 s. $\tau_1 = 784 \pm 402$ ms and $\tau_2 = 58 \pm 42$ ms, respectively. A fraction of the traces displayed a continuous and almost linear drift, yielding constants longer than the duration of the measurement. The latter were not included in the plots as the fits were under-constrained.

4.3.1 Recovery of Bundle Position

Immediately following cessation of the stimulus, the average bundle position was at an offset with respect to its resting position. We calculated this offset (X_0) from the fitted function (Eq. 4.1) for all available traces. A significant range in X_0 was observed across cells (∼100–600 nm). The size of X_0 was positively correlated with the duration of the imposed deflection (Fig. 4.4) at shorter step durations (T$<$ 5 s). More variation in the offset was observed at longer deflections, with some cells showing plateaus or non-monotonic dependence on stimulus duration.

As a measure of the dynamics of recovery, we determined the time required by the bundles to regain their steady-state positions. From the fitted function, this time (T_{ss}, see Materials and Methods) is taken as the time when the derivative of bundle motion first reaches -0.02 nm/ms. Figure 4.5 (A) shows the contour plot of the derivative of hair cell motion for a series of recordings taken after step

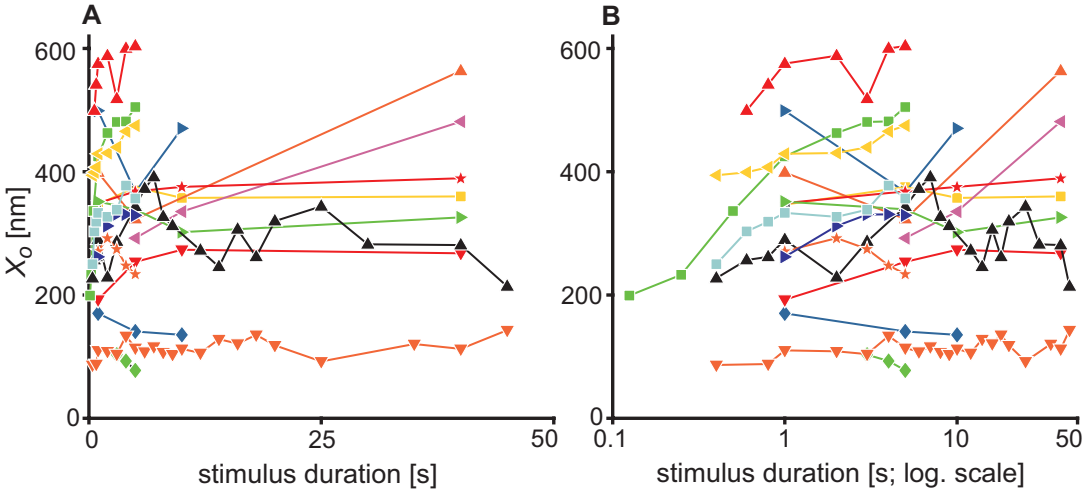

Figure 4.4: Offset after overstuimulation. (A) Xo (defined as X(end)-X(0), where X(t) is the sum of two exponentials fitted to the recording) as a function of stimulus duration for 17 different cells. Cell are represented by separate symbols. Results are shown for all the traces which yielded a good fit. (B) Same as (A), but using a logarithmic abscissa.

stimuli of fixed amplitude and varying duration. The plot demonstrates that the return to the steady-state position decreased with decreasing stimulus duration and increased when the stimulus was prolonged. Varying the threshold for T_{ss} did not qualitatively affect its dependence on stimulus duration. Similar results were observed for 16 other hair cells (Figures 4.5 (B),(C)): for short stimulus durations, T_{ss} rises sharply, with a subsequent leveling off when stimulus durations exceed ~ 5 seconds.

4.3.2 Recovery of Spontaneous Oscillations

All of the tested cells showed robust spontaneous bundle oscillations prior to stimulation. After the imposed deflection, the period over which the hair cells were quiescent varied systematically with the duration of the presented stimulus. As an example, Figure 4.6 (A) shows a series of traces from a single hair cell, obtained following deflections of different duration. As the length of the stimulus increased,

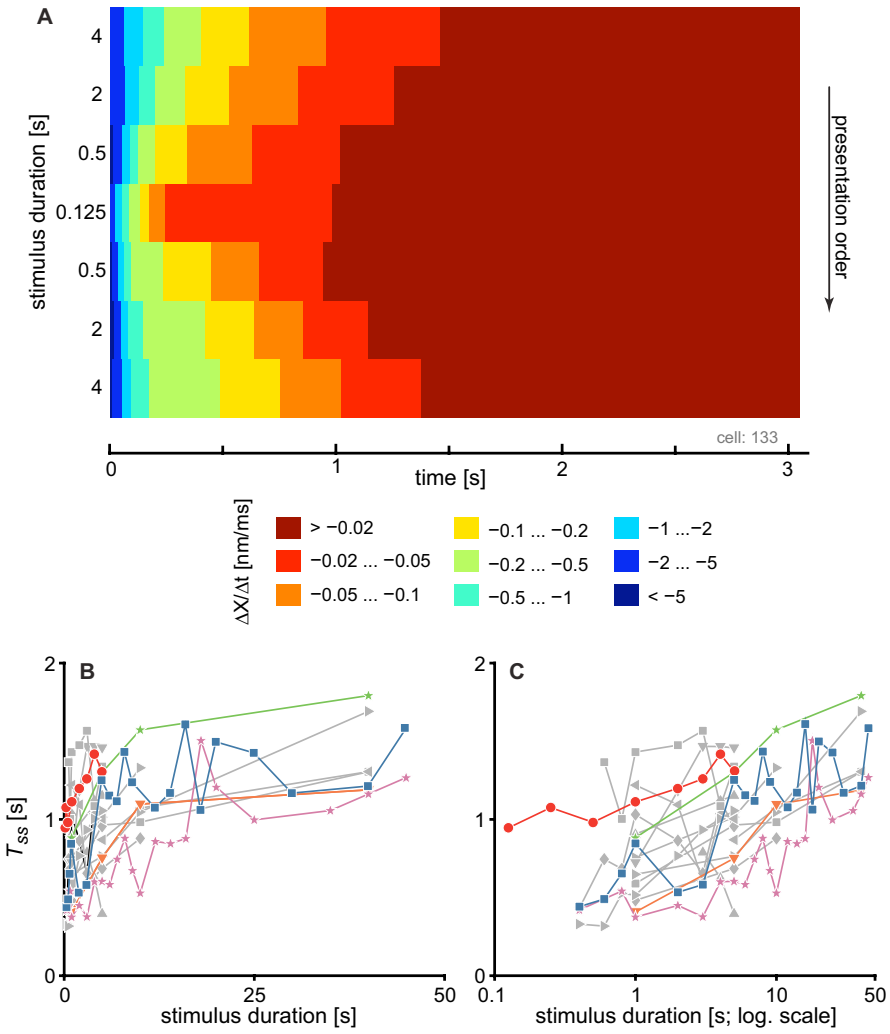

Figure 4.5: The time for the bundle to return to its steady-state position depends on stimulus duration. For a series of traces from a single cell, each recording was fitted with a sum of two exponentials. The derivatives of these fitted functions are represented in the form of a contour plot with slopes given in the legend (A). Rows give different stimulus durations, with the recording order from top to bottom. We arbitrarily chose 0.02 nm/ms as the threshold for steady-state, the similarity between different contours indicate that the results do not critically depend on the criterion value. (B) The time to reach steady-state (Tss) as a function of stimulus duration for 14 different cells. These cells each had recordings for at least 4 different stimulus durations. Cells are represented by separate lines/symbols. The thick gray line corresponds to the cell shown in (A). (C) Same as (B), but using a logarithmic abscissa.

the time at which the bundle resumed spontaneous oscillation (T_q) also increased. Note that subsequently decreasing the stimulus duration showed the opposite trend, indicating reversibility of the effect. While recovery was incomplete, with slower oscillations in subsequent recordings, the dependence of T_q on stimulus duration (red line in Figure 4.6 (B)) remained robust. Figures 4.6 (B)(C) show the dependence of T_q on the length of the imposed deflection for the 20 hair cells on which different stimulus durations were tested. A monotonic increase in the duration of the quiescent interval was observed, with a sharp rise from 0.1 to ~ 5 seconds of stimulus, and a more gradual increase with longer applied steps. Data could not be reliably obtained for durations above ~ 50 s, as damage was accrued. In conjunction with T_q, we also extracted the offset in the bundle's position at the time of first oscillation (X_q). This parameter was likewise affected by stimulus duration, with a more sensitive dependence at short deflections (Fig. 4.7).

We also quantified the dependence of quiescent interval on the magnitude of the stimulus. For 5 cells (82 recordings) a five-second stimulus was applied at various amplitudes (300–2100 nm) and the time to the first oscillation was determined. No systematic dependence of T_q was observed over this range of amplitudes (Fig. 4.8).

4.4 Role of Ca^{2+} in the Dynamics of Recovery

As prior work has shown that calcium plays a modulatory role in active hair bundle motility, we explored its effects on the duration of the quiescent interval induced by prolonged deflection. Figure 4.9 displays examples of measurements in which the hair bundle was deflected for a fixed interval of time (5 seconds), under conditions of varying calcium concentration in the surrounding medium. Decreasing the external calcium concentration led to slower spontaneous oscillations, consistent with prior results in the field. The quiescent interval (T_q) induced by the deflection

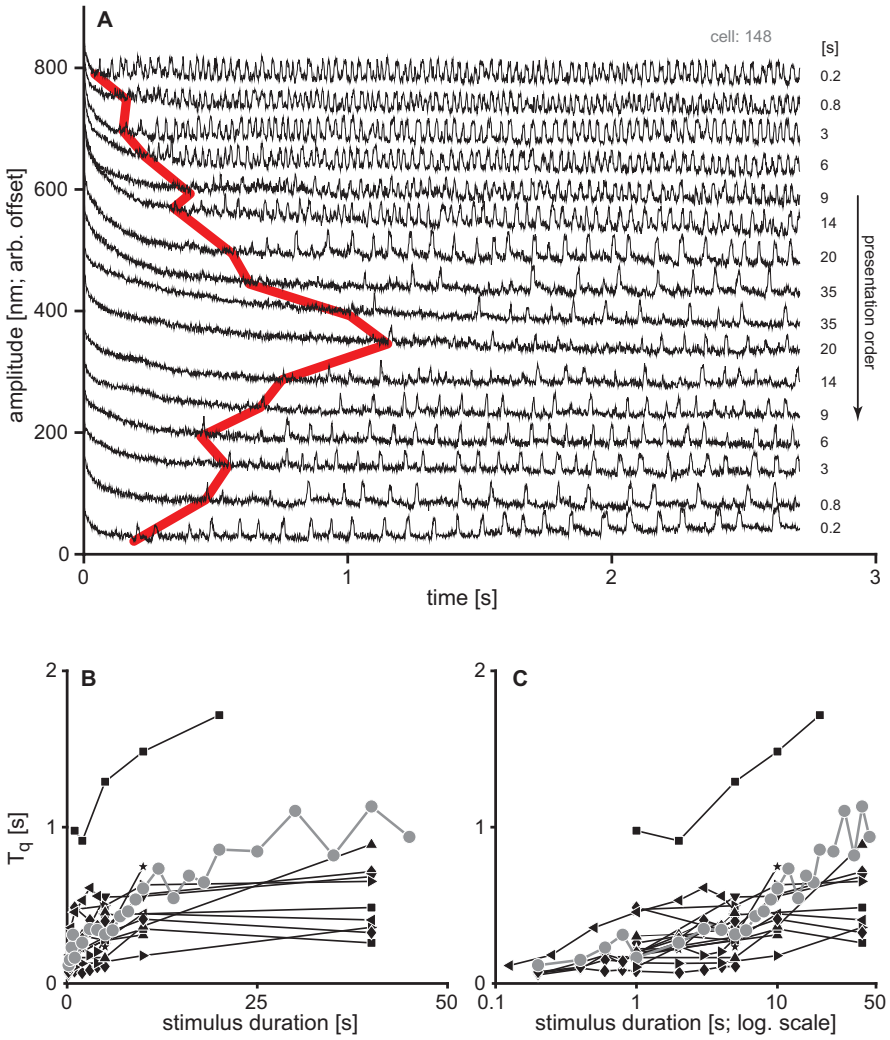

Figure 4.6: The time of the occurrence of the first bundle oscillation depends on stimulus duration. (A) Waterfall plot of a series of traces recorded from a single cell. Each trace was recorded following a stimulus of different duration (indicated on the right, in seconds), with the recording order from top to bottom. The thick red line connects the start of the first bundle oscillation Tq in each trace. (B) Tq as a function of stimulus duration, for 20 cells for which recordings at a minimum of two different stimulus durations were available. Cells are represented by different symbols. The thick gray line corresponds to the cell shown in (A). (C) Same as (B), but plotted on a logarithmic abscissa

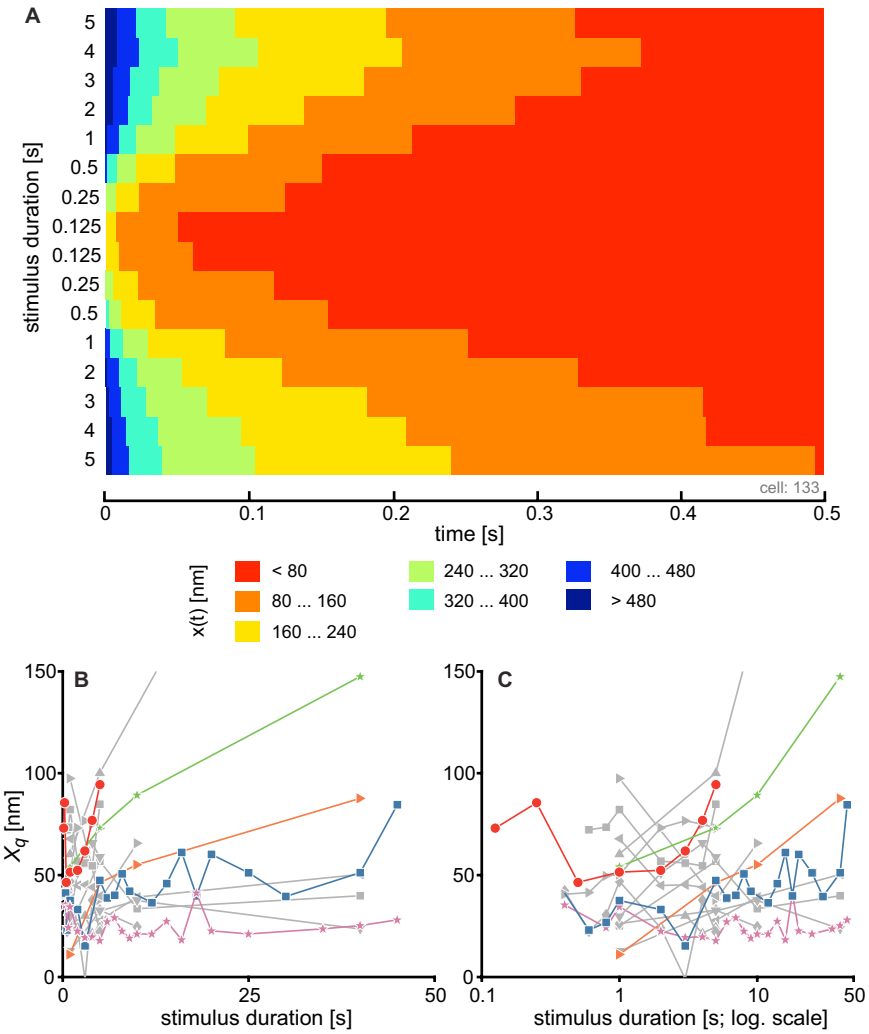

Figure 4.7: Offset in the position of the hair bundle position does not determine its dynamic state. For a series of traces obtained from a single cell, the bundle's position, with respect to that at the end of the recording is represented in the form of a contour plot (A). Different rows correspond to different stimulus durations, with the recording order displayed from top to bottom. (B) Xq as a function of stimulus duration was obtained for 17 different cells for which recordings at a minimum of two different stimulus durations were available. Cells are represented by a different symbols. The thick gray line corresponds to the cell shown in (A). (C) Same as (B), but plotted on a logarithmic abscissa.

was shorter, recovering more rapidly post stimulus cessation (Figure 4.10). Return to the original ionic conditions raised the frequency of oscillation; complete recovery of original oscillation was, however, seldom observed. Overstimulation in the presence of higher calcium concentration was detrimental to the hair cells, with increased variability and only a partial recovery upon return to baseline calcium conditions. We hence focus on effects of decreasing the external calcium concentration.

Figure 4.10 shows the intervals of induced quiescence (T_q) versus calcium concentration in the surrounding medium for multiple cells. Data are included only if obtained from hair bundles that displayed eventual recovery to the oscillatory state. T_q values and hard to quantify for high calcium data, which can be seen in Figure 4.9. T_q has a clearer relation on extracellular calcium for calcium concentration lower than 250μM. As another measure of the effect of calcium, additional experiments were done in the presence of carboxyeosin diacetate (CEDA) in the external medium, as shown in Figure 4.11. CEDA blocks the calcium extrusion pumps that are involved in maintaining the calcium concentration within the stereocilia. Inhibition of the extrusion pumps intensified the effects of overstimulation, prolonging the suppression of oscillation post stimulus. The effect was however convolved with irreversible rundown of the active bundle motility in the presence of the blocker.

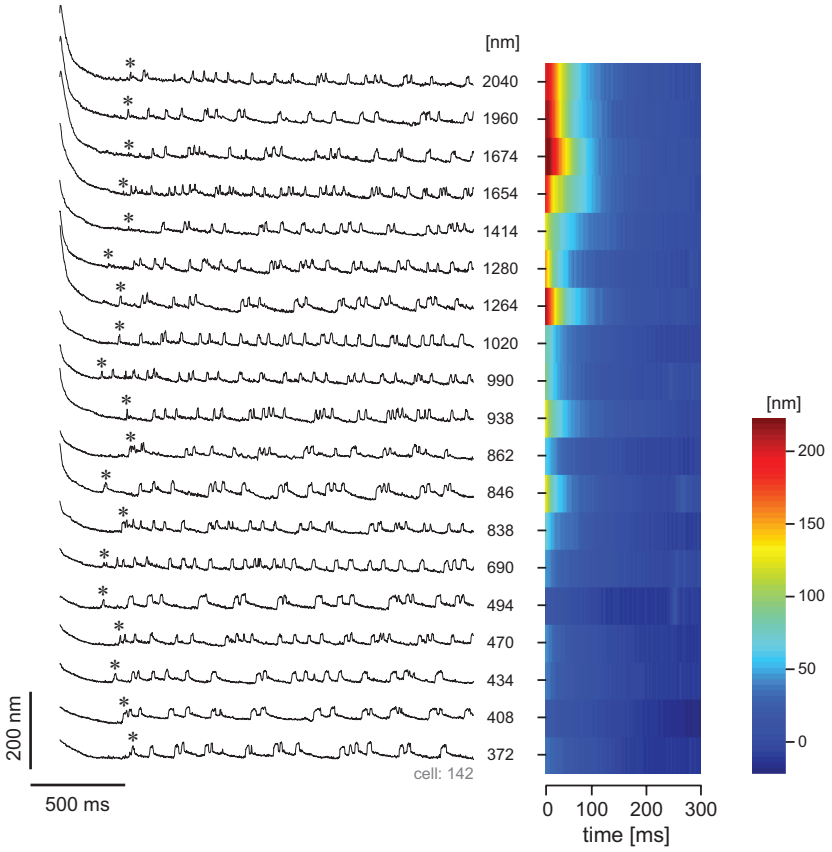

Figure 4.8: (A) Hair bundle motion recoverd after stimuli of fixed duration (5 seconds), at various amplitudes of deflection. Numbers on the right indicate stimulus amplitudes in nanometers. (B) A contour plot of the bundle position indicates that the time at which the bundle regains its steady state position is affected only weakly by the imposed deflection.

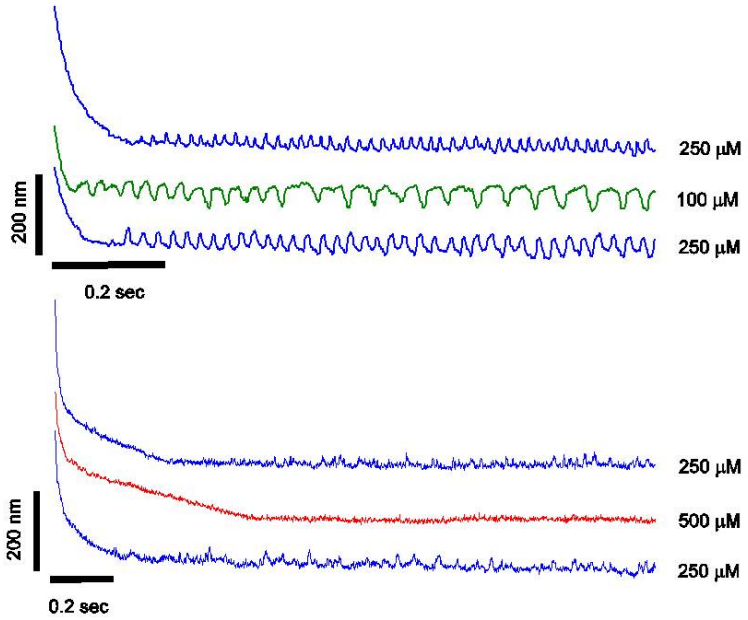

Figure 4.9: Hair bundle motion for a single hair cell was recorded under different concentrations of calcium in the surrounding endolymph solution. Duration of the imposed deflection was kept constant at 5 seconds for all of the recordings. From these two sets of recordings we can see that the adaptation and recovery of hair bundle position is faster in lower calcium solutions.

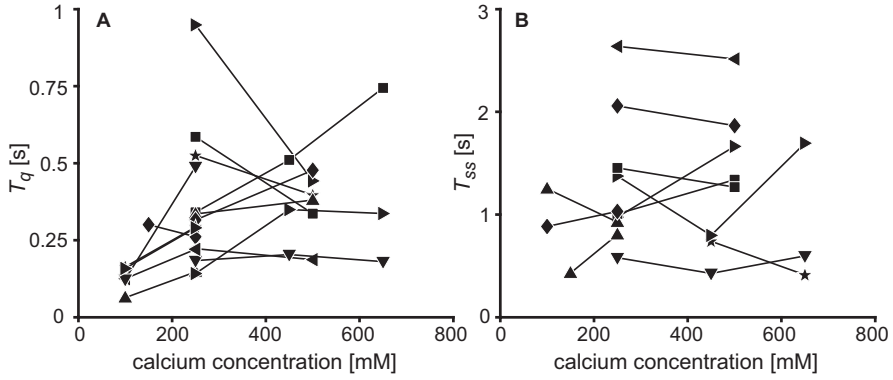

Figure 4.10: Hair bundle motion for a multiple hair cells were recorded under different concentrations of calcium in the surrounding endolymph solution. Duration of the imposed deflection was kept constant at 5 seconds for all of the recordings. Tq (A) and Tss (B) were determined for 15 cells.

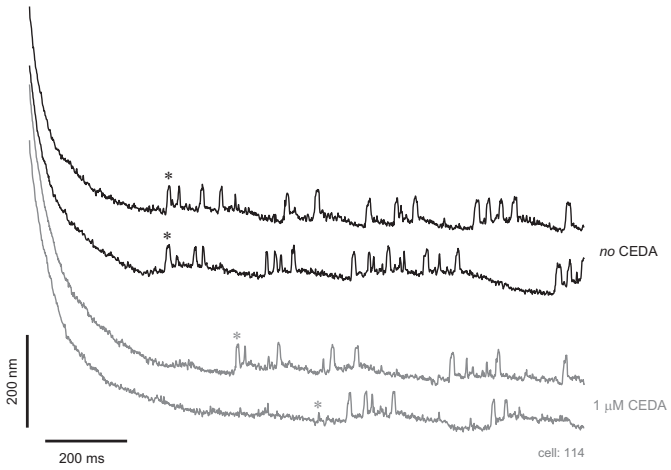

Figure 4.11: Top two traces represent hair bundle motion recorded post 5 second stimulation. Bottom two traces were recorded under the same conditions with addition of 1 μM CEDA, a known blocker of calcium extrusion pumps. We consistently observed an increase in the time of recovery Tq with the addition of CEDA into the solution.

CHAPTER 5

Conclusion

To assess the effects of overstimulation on the dynamic state of a hair bundle, we imposed prolonged high-amplitude deflections and measured the subsequent recovery. Our measurements revealed two main effects, an induced offset in the resting position of the bundle and temporary suppression of the innate oscillation. Both effects could persist for seconds after the stimulus and showed a dependence on the stimulus duration.

Relaxation of the hair bundle to its equilibrium position following cessation of the stimulus exhibited a complex temporal profile. Fitting the data with two exponentials allowed us to extract the timescales characterizing the motion with no a priori assumptions as to the biochemical identity of the adaptation mechanisms. The excellent fit of this function to the data implies the existence of two processes that operate on very different time scales.

Multiple adaptation mechanisms have been demonstrated in hair cells of the inner ear. Myosin motors enable a tension-sensitive adaptation, by climbing and slipping along the actin core of the stereocilia [22]. The shorter time constant that we observed ($\tau_2 = 58 \pm 42$ ms; Fig. 3) is consistent with that expected for myosin-based adaptation in the bullfrog sacculus. The initial slope of the recovery, however, indicates climbing speeds significantly higher than those previously reported for myosin 1C [48]. The initial recovery therefore may reflect signatures of a fast adaptation process [6], also mediated by the myosin motors [26] or caused by an additional relaxation element [7]. For the longer time constant ($\tau_1 = 784 \pm 402$

ms; Figure 4.3), we recently proposed the existence of a variable gating spring with a calcium-dependent stiffness [53]. This element was hypothesized to exhibit dynamics that are slow with respect to the myosin-based adaptation. The slow dynamics of recovery measured in these experiments are consistent with those of the variable gating spring proposed in the model. Across the recordings, the two time constants were correlated (correlation coefficient = 0.47), indicating that the two mechanisms are not independent.

As the slower adaptation mechanism was affected by calcium, its time constant may reflect the relatively slow dynamics of calcium pumps within the stereocilia [58]. During stimulus presentation, the transduction channels are kept in a preferentially open state for a prolonged period of time, during which calcium could accumulate within the stereocilia. After cessation of the stimulus, the slow extrusion of calcium by these pumps would gradually restore the concentration to the internal resting level. The accumulated internal calcium could also affect myosin-based adaptation, an internal relaxation element, and opening probability of the ion channels, thus affecting the faster time scale as well.

Apart from the observed relaxation of the hair bundle's position, the second striking effect of high-amplitude mechanical deflection was to induce a temporary crossover from the oscillatory to the quiescent state. Theoretical models of hair bundle motility have proposed that it can exhibit a stable limit-cycle oscillation, or operate in a regime where it amplifies but remains quiescent in the absence of input [20]. The bifurcation between these regimes is under control of an internal parameter, which has been proposed to be modulated by a feedback mechanism. In a recent study, we modeled hair bundle dynamics as a system poised near a subcritical Hopf bifurcation [56], with bistable switching between oscillation and quiescent state. A feedback equation on the control parameter maintains it near the bifurcation in the oscillatory regime. In the model, a strong stimulus can shift the control parameter across the bifurcation point, which leads to suppression

of spontaneous oscillation. The feedback equation then describes the subsequent recovery of the control parameter to its original value, returning the bundle to its oscillatory state.

The time required for recovery to the oscillatory state (T_q) was observed to be sensitively dependent on the duration of the applied stimulus (Figure 4.6). This finding is consistent with the proposed notion of dynamic feedback on the control parameter. As longer stimuli would lead to further detuning of the parameter, the system would exhibit a slower subsequent recovery. Stimulus duration also affects the offset in the bundle position (Figure 4.4), which constitutes one of the candidates of the control parameters. Offset alone, however, does not explain all of the experimental observations. First, variation in the stimulus amplitude, which results in varying initial offsets, has little effect on the timing of the recovery of bundle oscillations (T_q; Figure 4.7). Second, variation in the external calcium concentration (Figure 4.10) or the application of calcium pump blockers (Figure 4.11) exert an effect on T_q, without significantly changing the dynamics of position recovery. The data indicate that in addition to the induced offset, calcium plays a direct role in modulating the dynamic state of the hair bundle. Extensive literature exists on the importance of calcium feedback in the dynamics of individual hair cells. Our experiments are consistent with this prevailing view.

The current study sheds light on how the hair bundle recover to its optimal performance after mechanical overstimulation. The myosin-based adaptation mechanism was pushed to the limit, revealing a less robust and slower feedback mechanism working on the order of seconds. It is possible to attribute the slow recovery motion purely to frictional forces between stereocilia or adhesive stereociliary proteins [35, 34]. However, for such explanations to work on the correct timescale, special conditions have to be met. In mammals, acoustic overstimulation was found to increase calcium concentration in hair cells [25], suggesting a universal feedback mechanism with PMCA pump/variable gating spring playing a

central role. A peripheral gain control which adapts to the incoming signal could enhance the robustness of the hair cell sensitivity and protect it against accrued damage.

References

[1] N Adamek, L Coluccio, and M Geeves *Calcium sensitivity of the cross-bridge cycle of Myo1C, the adaptation motor in the inner ear* PNAS 105:5710-5715 (2008)

[2] C Armstrong and W Roberts *Electrical Properties of Frog Sacclular Hair Cells: Distortion by Enzymatic Dissociation* J. Neurosci. 18(8):2962-2973 (1998)

[3] J Ashmore et al. *The remarkable cochlear amplifier* Hearing Research 266:1-17 (2010)

[4] J Assad, N Hacohen, and DP Corey *Voltage dependence of adaptation and active bundle movement in bullfrog saccular hair cells* PNAS 86:2918-2922 (1989)

[5] J Assad, G Shepherd, and D Corey *Tip-link integrity and mechanical transduction in vertebrate hair cells* Neuron 7:985-994 (1991)

[6] M Benser, R Marquis, and AJ Hudspeth *Rapid, Active Hair Bundle Movements in Hair Cells from the Bullfrog's Sacculus* J. Neurosci. 16(18):5629-5643 (1996)

[7] D Bozovic and AJ Hudspeth *Hair-bundle stiffness elicited by transpithelial electrical stimulation of hair cells in the sacculus of the bullfrog* PNAS 100(3):958-963 (2003)

[8] M Beurg et al. *The actions of calcium on hair bundle mechanics in mammalian cochlear hair cells* Biophys J 94(7):2639-2653 (2008)

[9] M Beurg, R Fettiplace, JH Nam, and AJ Ricci *Localization of inner hair cell mechanotransducer channels using high-speed calcium imaging* Nature Neurosci. 12:553-558 (2009)

[10] M Beurg, JH Nam, Q Chen, and R Fettiplace *Calcium balance and mechanotransduction in rat cochlear hair cells* J Neurophysiol 104:18-34 (2010)

[11] W Bialek *Physical limits to sensation and perception* Ann. Rev. Biophys. Biophys. Chem. 16:5-78 (1987)

[12] S Camalet et al. *Auditory sensitivity provided by self-tuned critical oscillation of hair cells* PNAS 97(7):3183-3188 (2000)

[13] M Castellano-Munoz, S Israel, and A J Hudspeth*Efferent Control of the Electrical and Mechanical Properties of Hair Cells in the Bullfrog Sacculus* PLoS One 5(10):13777 (2010)

[14] E Cheung and DP Corey *Ca^{2+} Changes the Force Sensitivity of the Hair-Cell Tranduction Channel* Biophys. J. 90:124-139 (2006)

[15] Y Choe, M Magnasco, and AJ Hudspeth *A model for amplification of hair-bundle motion by cyclical binding of Ca^{2+} to mechanical-transduction channels* PNAS 95:15321-15326 (1998)

[16] NP Cooper and WS Rhode *Basilar membrane mechanics in the hook region of cat and guinea-pig cochleae: Sharp tuning and nonlinearity in the absence of baseline position shifts* Hearing Research 63:163-190 (1992)

[17] AC Crawford and R Fettiplace *The mechanical properties of ciliary bundles of turtle cochlear hair cells* J Physiol 364(1):359-379 (1985)

[18] W Denk, J Holt, G Shepherd, and D Corey *Calcium Imaging of Single Stereocilia in Hair Cells: Localization of Transduction Channels at Both Ends of Tip Links* Neuron 15:1311-1321 (1995)

[19] P Dallos *The active cochlea* J Neurosci 12(12):4575-4585 (1992)

[20] Eguiluz et al. *Essential nonlinearities in hearing* Phys Rev Lett 84(22):5232-5235 (2000)

[21] R Eatock, DP corey, and AJ Hudspeth *Adaptation of Mechanoelectrical transduction in hair cells of the bullfrog's sacculus* J. Neurosci. 7:2821-2836 (1987)

[22] R Eatock *Adaptation in Hair Cells* Annu. Rev. Neurosci. 23:285-314 (2000)

[23] R Fettiplace and PA Fuchs *Mechanisms of Hair Cell Tuning* Annu. Rev. Physiol. 61:809-834 (1999)

[24] L Fredrcikson-Hemsing, S Ji, R Bruinsma, and D Bozovic *Mode-locking dynamics of hair cells of the inner ear* Phy. Rev. E 86:021915(2012)

[25] A Friberger, A Flock, M Ulfendahl, and B Flock *Acoustic overstimulation increases outer hair cell Ca^{2+} concentrations and causes dynamic contractions of the hearing organ* PNAS 95:7127-7132 (1998)

[26] P Gillespie and D Corey *Myosin and Adaptation by Hair Cells* Neuron 19:955-958 (1997)

[27] P Gillespie and J Cyr *Myosin-1C, the hair cell's adaptation motor* Annu. Rev. Physiol. 66:521-545 (2004)

[28] P Gillespie and U Muller *Mechanotransduction by hair cells: models. molecules, and mechanisms* Cell 139:33-44 (2009)

[29] J Howard and AJ Hudspeth *Mechanical relaxation of the hair bundle mediates adaptation in mechaelectrical tranduction by the bullfrog's saccular hair cell* PNAS 84:3064-3068 (1987)

[30] AJ Hudspeth *Making an Effort to Listen: Mechanical Amplification in the Ear* Neuron 59 (2008).

[31] J Holt, D Corey *Two mechanisms for transducer adaptation in vertebrate hair cells* PNAS 97(22):11730-11735 (2000)

[32] B Kachar, M Parakkal, and J Fex *Structural basis for mechanical transduction in the frog vestibular sensory apparatus: I. the otolithic membrane* Hearing Research 45:179-190 (1990)

[33] Kandel, Schwartz, and Jessel *Principles of Neural Science, 4th Edn.* Chp. 30-31

[34] K Karavitaki and D Corey *Sliding Adhesion Confers Coherent Motion to Hair Cell Streocilia and Parallel Gating to Transduction Channels* J. Neurosci. 30(27):9051-9063 (2010)

[35] A LeBoeuf, D O Maoileidigh, and AJ Hudspeth *Divalent counterions tether membrane-bound carbohydrates to promote the cohesion of auditory hair bundles* Biophy. J. 101:1316-1325 (2011)

[36] L Le Goff, D Bozovic, and AJ Hudspeth *Adaptive shift in the domain of negative stiffness during spontaneous oscillation by hair bundles from the internal ear* PNAS 102:16996-17001 (2005)

[37] MC Liberman, J Gao, D He, X Wu, S Jia, and J Zuo *Prestin is required for electromotility of the outer hair cell and for the cochlear amplifier* Nature 419:300-304 (2002)

[38] E Lumpkin, R Marquis, and AJ Hudspeth *The selectivity of the hair cell's mechanoelectrical transduction channel promotes Ca^{2+} flux at low Ca^{2+} concentrations* PNAS 94 10997-11002 (1997)

[39] E Lumpkin, AJ Hudspeth *Regulation of Free Ca^{2+} Concentration in Hair-Cell Streocilia* J. Neurosci. 18(16):6300-6318 (1998)

[40] M Ospeck, VM Eguiliz, and O Magnasco *Evidence of a Hopf Bifurcation in Frog Hair Cells* Biophy. J. 80:2597-2607 (2001)

[41] Manceva et al. *Calcium regulation of calmodulin binding to and dissociation from the myo1c regulatory domain* Biochemistry 46(42):11718-26 (2007)

[42] G Manley *Evidence for an active process and a cochlear amplifier in non-mammals* J. Neurophys. 86:541-549 (2001)

[43] R Marquis, and AJ Hudspeth *Effects of extracellular Ca2+ concentration on hair-bundle stiffness and gating spring integrity of hair cells* PNAS 94:11923-11928 (1997)

[44] P Martin and AJ Hudspeth *Active hair-bundle movements can amplify a hair cell's response to oscillatory mechanical stimuli* PNAS 96:14306-14311 (1999)

[45] P Martin, AD Mehta, and AJ Hudspeth *Negative hair-bundle stiffness betrays a mechanism for mechanical amplification by the hair cell* PNAS 97:12026-12031 (2000)

[46] P Martin, AJ Hudspeth, and F Julicher *Comparison of a hair bundle's spontaneous oscillations with its response to mechanical stimulation reveals the underlying active process* PNAS 98:14380-14385 (2001)

[47] P Martin and AJ Hudspeth *Compressive nonlinearity in the hair bundle's active response to mechanical stimulation* PNAS 98:14386-14391 (2001)

[48] P Martin, D Bozovic, Y Choe, and A J Hudspeth*Spontaneous Oscillation by Hair Bundles of the Bullfrog's Sacclulus* J. Neurosci. 23(11):4533-4548 (2003)

[49] M Mulroy et. al. *Gap Junctional connections between hair cell's supporting cells and nerves in a vestibular organ* Hearing Research 71:98-105 (1993)

[50] L Robles and MA Ruggero *Mechanisms of Mammalian Cochlea* Physiol. Rev. 81:1305-1352 (2001)

[51] M Ruggero and N Rich *Application of a commercially-manufactured Doppler-shift laser velocimeter to the measurement of basilar membrane vibration* Hear. Res. 51:215230 (1991)

[52] M Ruggero, N Rich, A Recio, S Narayan, and L Robles *Basilar-membrane responses to tones at the base of the chinchilla cochlea* J. Acoust. Soc. Am. 101:2151-2163 (1997)

[53] Y Roongthumskul, L Fredrickson, A Kao, D Bozovic *Multiple-Timescale Dynamics Underlying Spontaneous Oscillations of Saccular Hair Bundles* Biophys J 101:603-610 (2011)

[54] H Sakaguchi, J Tokita, U Muller, and B Kachar *Tip links in hair cells: molecular composition and role in hearing loss* Curr. Opin. Otolaryngol. Head Neck Surg. 18:388-393 (2009)

[55] G Shepherd and DP Corey *The extent of adaptation in bullfrog sacculus hair cells* J. Neurosci. 14:6217-6229 (1994)

[56] R Shlomovitz et al. *Low Frequency Entrainment of Oscillatory Bursts in Hair Cells* Biophys J 1046(42):11718-26 (2011)

[57] P Van Dijk, M Mason, R Schoffelen, P Narins, and SWF Meenderink *Mechanics of the frog ear* Hearing Research 273:46-58(2011)

[58] E Yamoah, et al. *Plasma Membrane Ca^{2+} -ATPase Extrudes Ca^{2+} from Hair Cell Streocilia* J. Neurosci. 18(2):610-624 (1998)

[59] J Zheng, W Shen, D He, K Long L Madison, and P Dallos *Prestin is the motor protein of cochlear outer hair cells* Nature 405:149-155 (2000)